Atherosclerosis 284 (2019) 110–120

Contents lists available at ScienceDirect

Atherosclerosis

journal homepage: www.elsevier.com/locate/atherosclerosis

Z-Ligustilide protects vascular endothelial cells from oxidative stress and rescues high fat diet-induced atherosclerosis by activating multiple *NRF2* downstream genes

Yao Zhu[a,b,1], Yajie Zhang[c,d,1], Xia Huang[e,f], Yong Xie[a,b], Yuan Qu[e,f], Hongyan Long[c,d], Ning Gu[f,*], Weimin Jiang[a,b,**]

[a] Department of Cardiology, The Affiliated Hospital of Nanjing University of Chinese Medicine, Nanjing, Jiangsu, PR China
[b] First clinical medicine college of Nanjing University of Chinese Medicine, Nanjing, Jiangsu, PR China
[c] Department of Central Laboratory, The Affiliated Nanjing Hospital of Nanjing University of Chinese Medicine, Nanjing, Jiangsu, PR China
[d] Department of Clinical Biobank, The Affiliated Nanjing Hospital of Nanjing University of Chinese Medicine, Nanjing, Jiangsu, PR China
[e] Nanjing University of Chinese Medicine, Nanjing, Jiangsu, PR China
[f] Department of Cardiology, The Affiliated Nanjing Hospital of Nanjing University of Chinese Medicine, Nanjing, Jiangsu, PR China

HIGHLIGHTS

- Nrf2 pathway protects vascular endothelium from oxidative stress *in vivo* and *in vitro*.
- Z-Ligustilide ameliorates high fat induced-atherosclerosis in *LDLR*$^{-/-}$ mice.
- Z-Ligustilide activates Nrf2 and its downstream genes containing the ARE element, in vascular endothelial cells.

ARTICLE INFO

Keywords:
Z-Ligustilide
Oxidative stress
Vascular endothelium
Atherosclerosis
Nrf2

ABSTRACT

Background and aims: Oxidative stress-induced endothelial dysfunction is considered to exert a vital role in the development of atherosclerotic coronary heart disease (CHD). NRF2 is a key transcriptional factor against oxidative stress through activation of multiple *ARE*-mediated genes. Z-Lig is derived from the *Ligusticum* species with antitumor, anti-inflammation and neuroprotection activities. However, the antioxidant potentials of Z-Lig on endothelial dysfunction and atherosclerosis have not been well elucidated. Therefore, in the present work, we appraise the cytoprotective property and anti-atherosclerosis effect of Z-Lig.

Methods: Potential NRF2 activators were screened and verified by luciferase reporter gene assay. The protein and mRNA levels of NRF2 and *ARE*-mediated genes, and GSH/GSSG level in EA.hy926 cells treated with Z-Lig were detected. The cytoprotective property of Z-Lig was assessed in the tert-butyl hydroperoxide (t-BHP)-evoked oxidative stress model. Cell viability and reactive oxygen species (ROS) levels in EA.hy926 cells were determined. An atherosclerosis model induced by HFD was used to determine the anti-atherosclerosis effect of Z-Lig in HFD-fed *Ldlr*-deficient mice.

Results: In vitro, 100 μM Z-Lig upregulated expressions of NRF2 and *ARE*-driven genes, promoted accumulation of nuclear NRF2 and unbound NRF2- KEAP1 complex in EA.hy926 cells. Furthermore, Z-Lig alleviated oxidative stress and cell injury caused by t-BHP via stimulation of the NRF2/*ARE* pathway. *In vivo*, intervention with

Abbreviations: Z-Lig, Z-Ligustilide; ROS, reactive oxygen species; Nrf2, nuclear factor-erythroid 2-related factor 2; Keap1, Kelch like-ECH-associated protein 1; CVD, cardiovascular diseases; CHD, coronary heart disease; ARE, antioxidant response element; GSH, reduced glutathione; GSSG, glutathione disulfide; GCLM, glutamate-cysteine ligase modifier subunit; GCLC, glutamate-cysteine ligase catalytic subunit; GS, glutathione synthetase; GR, glutathione reductase; GPX, glutathione peroxidase; GRX, glutaredoxin; TR, thioredoxin reductase; TRX, thioredoxin; PRX, peroxiredoxin; SOD, superoxide dismutase; CAT, catalase; t-BHP, tert-butyl hydroperoxide; MDA, malondialdehyde; HFD, high fat diet; HO-1, heme oxygenase-1; GST, glutathione S-transferase; NQQ1, NAD(P)H quinone oxidoreductase 1; DMSO, dimethyl sulfoxide; DCFH-DA, 2', 7'-dichlorodihydrofluorescein diacetate; DMEM, Dulbecco's Modified Eagle Medium; TG, triglyceride; TC, total cholesterol; LDL-C, low density lipoprotein cholesterol; HDL-C, high density lipoprotein cholesterol; UBM, high resolution ultrasound biomicroscopy; ORO, Oil Red O; OCT, optimum cutting temperature

* Corresponding author. Department of Cardiology, The Affiliated Nanjing Hospital of Nanjing University of Chinese Medicine, Naning, Jiangsu, PR China.
** Corresponding author. Department of Cardiology, The Affiliated Hospital of Nanjing University of Chinese Medicine, Nanjing, Jiangsu, PR China.
E-mail addresses: jsguning@163.com (N. Gu), jwm0410@163.com (W. Jiang).
[1] These authors contributed equally to this work.

https://doi.org/10.1016/j.atherosclerosis.2019.02.010
Received 12 October 2018; Received in revised form 14 January 2019; Accepted 5 February 2019
Available online 25 February 2019
0021-9150/

20 mg/kg Z-Lig markedly restrained atherosclerosis progression, including attenuation of HFD-induced atherosclerotic plaque formation, alleviation of lipid peroxidation and increase in antioxidant enzyme activity in aortas of HFD-fed *Ldlr* $^{-/-}$ mice. The chemopreventive effects of Z-Lig might be associated with the activation of NRF2 and *ARE*-driven genes.

Conclusions: The present study suggested that Z-Lig is an effective NRF2 activator, which can protect vascular endothelial cells from oxidative stress and rescue HFD-induced atherosclerosis.

1. Introduction

CVD is the leading cause of death around the world, with the mortality of 1/3 each year. Atherosclerotic lesion formation is considered the most prevalent cause of CVD. It is reported that about 7 million deaths throughout the world are caused by atherosclerotic coronary heart disease (CHD) annually [1–3]. Numerous studies have suggested that endothelial dysfunction induced by ROS is an initial step of atherosclerosis, which plays a key role in pathogenesis of atherosclerosis [4–6]. Oxidative stress is a condition in which overproduced ROS cannot be effectively scavenged by endogenous antioxidant defense systems. Excessive ROS will further perturb cell redox balance, with a shift toward an increased oxidative stress [7,8]. Thus, the potential impacts of natural antioxidants on the prevention of oxidative stress-induced atherosclerosis has been well recognized.

NRF2 is a transcriptional factor belonging to the leucine zipper family. NRF2 protects cells against oxidative stress challenge by activating multiple *ARE*-mediated genes [9–11]. Various phase II detoxifying enzymes are regulated via the NRF2/*ARE* signaling pathway, including *HO-1, GST, NQO1, GCLM, GR, GCLC, GS, GPX, GRX, TR, PRX, SOD, TRX* and *CAT* [12–14]. A Large amount of evidence has suggested that NRF2/*ARE* pathway promotes the cellular defenses against ROS-induced endothelial dysfunction by increasing the transcriptional activity of *ARE*-driven genes. These genes subsequently regulate the synthesis and metabolism of GSH, a well-known intracellular deoxidizer, and scavenge ROS directly or indirectly [15–17]. *Nrf2*$^{-/-}$ mice are more vulnerable to ROS-induced endothelial dysfunction and atherosclerosis, suggesting that *Nrf2* and downstream antioxidant genes exert a great effect on protecting endothelium against cytotoxic ROS [18,19]. It is reported that *Nrf2* specific knockout in bone marrow-derived cells could aggravate atherosclerosis in *Ldlr*$^{-/-}$ mice via stimulating foam cell formation and pro-inflammatory phenotype alteration [20].

Z-Lig, as one of the most abundant essential oils in the rhizomes of Ligusticum chuanxiong hort and Angelica sinensis (Oliv.) Diels, displays various pharmacological functions, such as antioxidant, anticancer, anti-inflammation, analgesia, vasodilatation, neuroprotection, etc [21–23]. Qi et al. reported that Z-Lig protected PC12 cells from oxidative damage and increased the intracellular content of GSH via upregulating Nrf2 expression. A recent study has demonstrated that Z-Lig attenuated oxidative stress in human keratinocytes caused by ultraviolet B via regulating NRF2/HO-1. It is also reported that Z-Lig alleviated cerebral ischemia by activating the Nrf2 pathway [24–26]. However, the antioxidant potential of Z-Lig on t-BHP-induced endothelial dysfunction and HFD-induced atherosclerosis has not been fully elucidated. Therefore, in the present work, we first explored the role of Z-Lig against cell damage caused by t-BHP in EA.hy926 cells. We also investigated the anti-atherosclerosis effect of Z-Lig in HFD-fed *Ldlr* $^{-/-}$ mice.

2. Materials and methods

2.1. Reagents

Z-Lig (purity > 98%) (CAS number: 4431-01-0, Cat. SMB00400, Sigma-Aldrich), DMSO, t-BHP, DCFH-DA, and MTT were bought from Sigma-Aldrich (St. Louis, MO, USA). Biochemical kits for TG, TC, LDL-C and HDL-C were obtained from Zhongsheng Bio-tech Company (Beijing, China).

2.2. Cell culture

The EA.hy926 cell line, originated from fusing human umbilical vein endothelial cells with A549 human lung carcinoma cells, was obtained from Shanghai Institute of Cell Biology (Shanghai, China). EA.hy926 cells were cultured in DMEM medium (Gibco, Grand Island, NY, USA) with 10% fetal bovine serum (Gibco), and 1% penicillin-streptomycin solution (Beyotime, Jiangsu, China). The cells were maintained in 10-cm plates.

2.3. MTT assessment

MTT assay was applied to measure cell viability. EA.hy926 cells were planted at a density of 5000 cells/dish into 96-well plates. The specific experimental steps were previously described [16]. Cell viability was expressed as a percentage of the vehicle.

2.4. Cell transfection and luciferase report gene assay

The pGL4.37 [*luc2P/ARE/Hygro*] Vector purchased from Promega (Madison, WI, USA) was used to access *ARE* activation in EA.hy926 cells treated with or without Z-Lig. The pGL4.75 Vector [*hRluc/CMV*] (encoding Renilla luciferase) obtained from Promega was used as a normalization control. Briefly, 1×10^4 cells were plated in 96-well plates and incubated for 24 h. The pGL4.37 plasmid and pGL4.75 plasmid were co-transfected in EA.hy926 cells based on the instructions of Lipofectamine® 3000 Transfection Reagent (Invitrogen, Grand Island, NY, USA). After transfection for 24 h, cells were treated with DMSO or 1–100 μM Z-Lig for different time points, followed by detection using Dual-Glo® Luciferase Assay System (Promega) with a luminometer (GloMax 20/20n; Promega). Relative firefly luciferase intensity was normalized to Renilla luciferase intensity and the intensity was expressed as fold changes after Z-Lig intervention compared with the vehicle.

2.5. Real-time polymerase chain reaction (Real-time PCR)

EA.hy926 cells were washed with PBS for three times. The total RNA of EA.hy926 cells was extracted with TRIzol reagent (Invitrogen). The specific steps for reverse transcription and fluorescence quantitative were previously described [16]. Primers used for Real-time PCR were obtained from GENEray Biotechnology (Shanghai, China), and listed in Supplementary Table 1.

2.6. Western blotting

The protein from cells and aortas was extracted by RIPA lysis buffer (Beyotime). The specific experimental steps were previously described [16]. Primary antibodies used in this study were listed in Supplementary Table 2 and the second antibodies were purchased from Abcam (Cambridge, UK).

2.7. Co-immunoprecipitation

1×10^9 cells were harvested after treatment with 0 or 100 μM Z-Lig for 24 h. 1000 μL of whole cell lysate was collected to determine the protein concentration. Dynabeads™ Protein G Immunoprecipitation Kit (Thermo Fisher) and anti-KEAP1 antibody (5 μg, sc-365626, Santa Cruz) or control rabbit IgG was incubated following the protocols. Subsequently, the prepared beads-capture antibody complex and 1000 μg of protein lysate were incubated and gently shaken at 2–8 °C for 12 h to capture KEAP1 binding protein complex. After Co-IP procedures and native elution, samples were treated with 2 × SDS loading buffer and boiled to 100 °C for 5 min. SDS-PAGE and Western blotting were used for immunoblotting. Primary antibodies used in the experiment were anti-KEAP1 rabbit polyclonal antibody (1:1000, ab218815, Abcam) and anti-NRF2 rabbit polyclonal antibody (1:2000, sc13032, Santa Cruz).

2.8. Nuclear and cytosolic fractions

Nuclear and cytosolic fractions were obtained following manufacturer's protocols (Thermo Fisher, Catalog number: 78833). The specific experimental steps were previously described [16].

2.9. ROS detection

For ROS detection, EA.hy926 cells were pre-treated with Z-Lig for 24 h, and incubated with 200 μM t-BHP for another 6 h. After being washed with PBS for three times, EA.hy926 cells were stained with 10 μM DCFH-DA for half an hour in the dark. After being washed for three times with PBS, DCF fluorescence was determined with a flow cytometer (FC500, Beckman Coulter, California, Brea, USA).

2.10. GSH and GSSG determination

Content of GSH and GSSG in the EA.hy926 cells, serum and aortas of *Ldlr* $^{-/-}$ mice was assayed using the Total-Glutathione Detection Assay Kit (A061-1, Nanjing Jiancheng Bioengineering Institute, Nanjing, China) following the manufacturer's instructions. Fluorescence intensity was detected using a microplate reader (Bio-Tek) at the wavelength of 405 nm. GSH content = total GSH content – 2 × GSSG content.

2.11. NRF2-siRNA transient transfection

EA.hy926 cells were plated in 40-mm dishes. After cell confluence was up to 80%, *NRF2*-specific short interfering RNA (siRNA) was applied to downregulate *NRF2* expression (RIBOBIO, Guangzhou, China). A scramble siRNA was used as negative control (RIBOBIO). The specific experimental steps were previously described [16].

2.12. Experimental mice

Animal experiments complied with the National Institutes of Health Guidelines for the Use of Laboratory Animals. All experiments were authorized by the Jiangsu Animal Experimental for Medical and Pharmaceutical Research Center (Nanjing, Jiangsu, China). 45 male 7-week-old *Ldlr* $^{-/-}$ mice (C57BL/6JNju) weighing 17–22g were obtained from Nanjing Biomedical Research Institute of Nanjing University (Nanjing, China). Mice were accommodated to the laboratory environment for one week before the experiment. 45 mice were randomly divided into three groups, namely standard chow diet (STD) group, HFD group, and Z-Lig-treated group, with 15 in each of them. Mice in the STD group were fed a with standard chow diet, whereas mice in the HFD group and Z-Lig-treated group were fed a high fat diet (1.25% cholesterol, 40% fat) for 8 weeks (D12108, Research Diets, Inc). 3% (w/v) polysorbate 80 (TW-80) was used as vehicle to dissolve Z-Lig. Mice in the Z-Lig-treated group received intraperitoneal injection of 20 mg/kg Z-Lig once a day for 8 weeks, whereas mice in the other groups were administrated with the same volume of vehicle. Food intake and body weight were observed per week. UBM was performed at the 8th week of the experiment. After ultrasound assessment and 12 h of fasting, mice were sacrificed by overdose isoflurane exposure. The blood samples and tissues were collected for further analysis.

2.13. UBM detection

At week 8, micro-ultrasound imaging of the aortic arch plaques was conducted in 5 randomly chosen mice from each group. Before UBM detection, mice were anesthetized with isoflurane. The chest hair of mice was shaved and ultrasound transmission gel was used to ensure optimal image quality. UBM was conducted using a high resolution *in vivo* micro-imaging system (Vevo 2100 system, Visualsonics, Toronto, Canada). We applied a long axis view to observe the lesion of the aortic arch on B-mode. The measured plaques of aortic arch were at the origin of the brachiocephalic artery.

2.14. Serum lipid profile measurement

We obtained blood samples by cardiac puncture. After centrifugation for 10 min at 3000 × *g* at 4 °C, the serum was collected and frozen at −80 °C until use. Serum lipid profiles were assayed following manufacturer's instruction.

2.15. Evaluation of atherosclerotic plaques

After 8-week Z-Lig or vehicle intervention, the entire aorta, from ascending aorta to renal artery, was separated and immediately fixed using 4% paraformaldehyde. The separated aortas underwent an ORO (Sigma) staining for analysis of the lesion area. The levels of atherosclerotic plaque were described as percent of the positive plaque area from the whole aorta. To determine the sinus lesions in aortic root, hearts and aortic arches were embedded in OCT compound (Sigma), and frozen at −80°C for the following procedures. Serial sections (10 μm) were sliced with a Leica cryostat (Leica, Heidelberg, Germany). We stained the frozen sections with ORO and the lesion area were quantified using Image-Pro Plus (Media Cybernetics, USA).

2.16. Determination of serum and aortic oxidative stress

Activities of MDA (A003-1), Cat (A007-1), Gpx (A005-1) and Sod (A001-1) in mouse serum and aorta tissues were determined with commercial kits (Jiancheng) on the basis of manufacturer's protocols as previously described [27]. Briefly, Cat activity was measured by the absorbance of the yellow H_2O_2-ammonium molybdate complex at the wavelength of 405 nm (Definition of serum activity of Cat: 1 μmol H_2O_2 decomposing per ml blood serum (or plasma) per second is considered as 1 activity unit (U); Definition of Cat activity in tissue homogenate: 1 μmol H_2O_2 decomposing per mg tissue protein per second is considered as 1 activity unit (U)). Gpx activity was measured on the basis of reaction with dithio-dinitrobenzoic acid and calculation of GSH consumption by measuring absorbance at the wavelength of 412 nm (Serum Gpx activity definition: Reaction at 37 °C for 5 min, 1 μmol/L GSH concentration reduction (effect of nonenzymatic reaction is already deducted) in reaction system per 0.1 ml blood serum is considered as 1 enzyme activity unit (U); Definition of Gpx activity in tissue homogenate: 1 μmol/L GSH concentration reduction (effect of nonenzymatic reaction is already deducted) in reaction system per mg protein per minute is considered as 1 enzyme activity unit (U)). Sod activity was measured the absorbance at the wavelength of 550 nm based on the xanthine oxidase method (Definition of serum activity of Sod: One Sod activity unit is defined as 1 ml serum among which the inhibition rate of Sod is 50%; Definition of Sod activity in tissue

homogenate: One Sod activity unit is defined as 1 mg tissue protein among which the inhibition rate of Sod is 50%).

2.17. Immunofluorescence staining

EA.hy926 cells and frozen sections were fixed in 4% paraformaldehyde for 15 min. Subsequently, cells and sections were rehydrated in PBS for 10 min, soaked in 0.2% TritonX-100 at 37 °C for half an hour, and washed with PBS for three times. We blocked the frozen sections and cells with 5% goat serum for 60 min and incubated with anti-GAPDH, anti-Nrf2, anti-Cd31 and anti-Ho-1 at 4 °C for 12 h. After that, the frozen sections and cells were incubated with the polyclonal Alexa Fluor® 488 goat anti-rabbit IgG (#ab150077, Abcam, Cambridge, UK,1:500 dilution) and polyclonal Alexa Fluor® 594 goat anti-mouse IgG (#ab150116, Abcam, Cambridge, UK,1:500 dilution) for 90 min at 37 °C. Nuclei was stained with DAPI (#C1002, Beyotime, 1:1000 dilution). The images stained with Alexa Fluor® 488 represent Nrf2 and Ho-1, while those stained with Alexa Fluor® 594 were Cd31 and Gapdh. Images were randomly selected and analyzed using a confocal scanning laser microscope Zeiss LSM 710 (Carl Zeiss Microscopy GmbH, Jena, Germany).

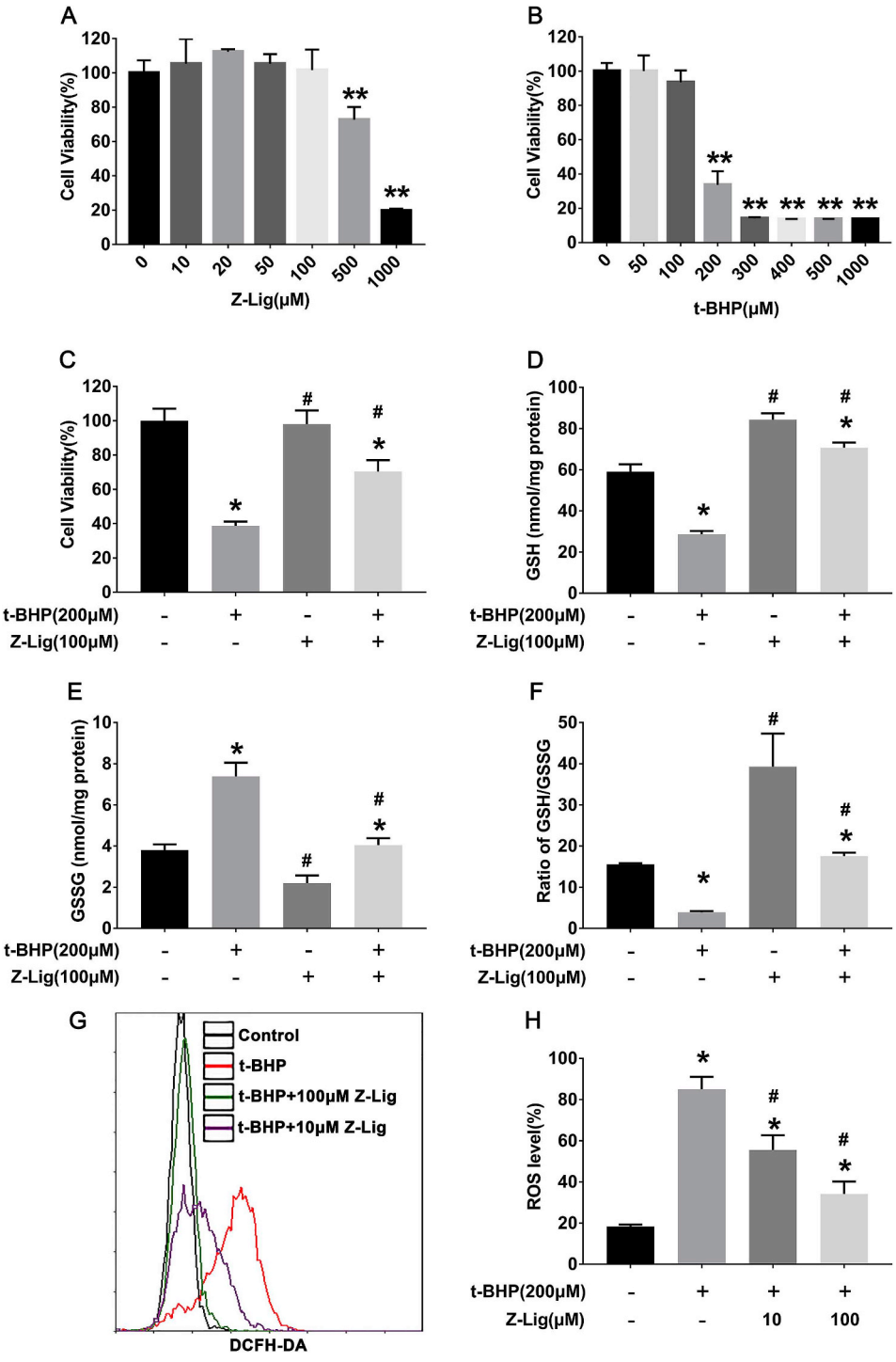

Fig. 1. Z-Lig protected against cytotoxicity induced by oxidative stress and increased intracellular GSH in EA.hy926 cells.
(A) Impacts of various concentrations of Z-Lig on cell viability of EA.hy926 cells. EA.hy926 cells were incubated with various concentrations (10–1000 μM) of Z-Lig for 24 h. Cell viability was assayed by MTT, and viability of EA.hy926 cells without any intervention was considered as 100%. (B) Effects of various concentrations of t-BHP on cell viability of EA.hy926 cells. EA.hy926 cells were incubated with various concentrations (50–1000 μM) of t-BHP for 6 h. Cell viability was assayed by MTT, and viability of EA.hy926 cells without any intervention was considered as 100%. (C–H) EA.hy926 cells were pretreated with 10 or 100 μM Z-Lig for 24 h, and then incubated with 200 μM t-BHP for another 6 h. (C) Z-Lig inhibited EA.hy926 cells from cell injury caused by t-BHP. Cell viability was assayed by MTT, and viability of EA.hy926 cells without any intervention was considered as 100%. (D–F) Effects of Z-Lig on the levels of intercellular GSH, GSSG and the ratio of GSH/GSSG in EA.hy926 cells. The levels of intercellular GSH, GSSG and the ratio of GSH/GSSG were measured following the protocol. (G) Flow cytometry detection of intercellular ROS. EA.hy926 cells were incubated with 10 μM DCFH-DA in serum-free medium for half an hour. DCF fluorescence intensity was measured with a flow cytometer. (H) Quantification of DCF fluorescence intensity (n = 3). Data are presented as means ± SD. $^{*}p < 0.05$ and $^{**}p < 0.01$ *vs.* untreated EA.hy926 cells. $^{\#}p < 0.05$ *vs.* t-BHP-intervened EA.hy926 cells.

2.18. Immunohistochemistry

Expressions of Nrf2, Ho-1, Gclc, Gclm, Sod1 and 4-Hne in vascular endothelium of *Ldlr* $^{-/-}$ mice were also evaluated by immunohistochemistry. Briefly, frozen sections were fixed overnight in 4% paraformaldehyde. After antigen retrieval and treatment with H_2O_2 for 20 min, sections were blocked for 1 h at room temperature with 5% bovine serum albumin in PBST. One section was incubated with Cd31 and the other section from the same sample was stained with another primary antibody (Supplementary Table 2) for 12 h at 4 °C, followed by HRP Detection System (Beyotime, Jiangsu, China) for 60 min at 37 °C. The sections were treated with DAB substrate (Beyotime) for 10 min. Hematoxylin staining solution was used for counterstain in nucleus for 4 min. Stained sections were scanned and digital hole slide images were performed using a digital slide scanner (Pannoramic 250/MIDI, 3D Histech Ltd, Budapest, Hungary). Hole slide images were visualized by the CaseViewer (Version 2.0, 3D Histech Ltd). Cd31 and another primary antibody on the different serial sections were captured in the same location to determine the expressions of Nrf2, Ho-1, Gclc, Gclm, Sod1 and 4-Hne in vascular endothelium.

2.19. Statistical analysis

GraphPad Prism 7.0 (GraphPad Software Inc., San Diego, CA, USA) was applied to analyze the data. We used one-way ANOVA to compare among different groups. Values were described as mean ± SD. $p < 0.05$ indicated statistical significance.

3. Results

3.1. Z-Lig exhibited preventive effects on oxidative stress-induced cytotoxicity and increased intracellular GSH in EA.hy926 cells

Z-Lig effects on cell viability of EA.hy926 were assayed by MTT. Incubation with 10–100 μM Z-Lig for 24 h had no effect on viability of EA.hy926 cells, while 500–1000 μM Z-Lig remarkably impaired the viability of EA.hy926 cells (Fig. 1A). Intracellular ROS levels were determined using flow cytometer analysis. The levels of intracellular ROS were significantly elevated under t-BHP incubation for 6 h. However, this was effectively restrained by Z-Lig pretreatment (Fig. 1G and H). MTT was used to examine the effects of Z-Lig on protecting EA.hy926 cells from cellular damage caused by t-BHP. As shown in Fig. 1B and C, incubation with t-BHP significantly reduced cell viability, which was dramatically restored by Z-Lig pretreatment. The effects of Z-Lig and t-BHP on the changes in GSH/GSSG content were also determined in EA.hy926 cells (Fig. 1D–F). Incubation with 100 μM Z-Lig for 24 h significantly promoted GSH biosynthesis and suppressed GSSG production, leading to an increase in GSH/GSSG ratio. Moreover, pretreatment with 100 μM Z-Lig for 24 h could attenuate the decreased GSH content and increased GSSG level under 200 μM t-BHP treatment, thereby elevating the ratio of GSH/GSSG.

3.2. Z-Lig intensively stimulated ARE-driven luciferase activities and NRF2 nuclear accumulation in EA.hy926 cells

EA.hy926 cells were co-transfected with a reporter plasmid

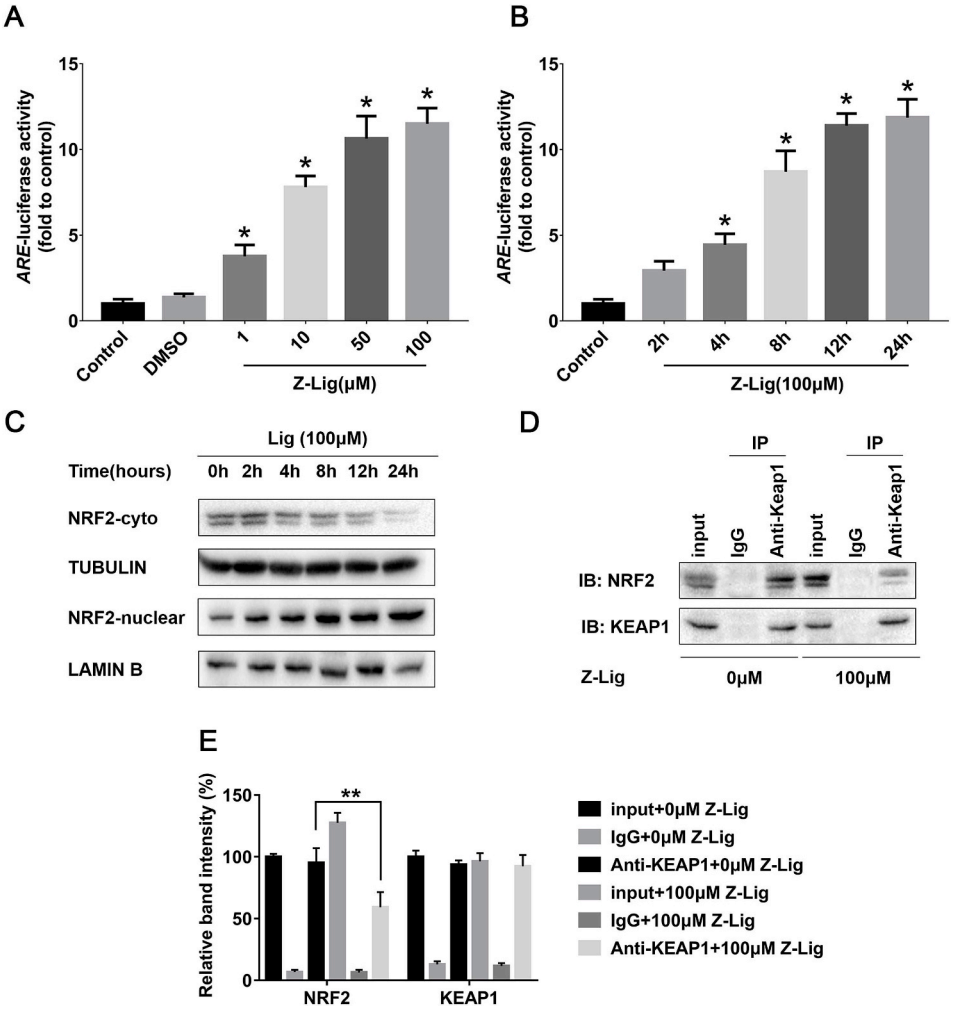

Fig. 2. Z-Lig intensively stimulated *ARE*-luciferase activity, promoted NRF2 nuclear accumulation and unbound NRF2-KEAP1 complex in EA.hy926 cells.
(A and B) Impact of Z-Lig on *ARE*-luciferase activity. Cells were co-transfected with a reporter plasmid and a control plasmid. After co-transfection, EA.hy926 cells were treated with DMSO for 24 h or Z-Lig (1–100 μM) for 24 h (A), or treated with 100 μM Z-Lig for 2, 4, 8, 12, 24 h (B) and then luciferase activity was determined (n = 3). Values are shown as mean ± SD. $^{*}p < 0.05$ *vs.* vehicle control. (C) Z-Lig promoted accumulation of nuclear NRF2. EA.hy926 cells were treated with 100 μM Z-Lig for 2, 4, 8, 12, 24 h, respectively. Nuclear and cytosolic fractions were obtained as described previously. Western Blotting was applied to detect protein expression of NRF2 in nucleus and cytoplasm. (D and E) Z-Lig promoted unbinding of KEAP1-NRF2 complex. EA.hy926 was treated with 0 or 100 μM Z-Lig for 24 h. IP: KEAP1, IB: KEAP1, NRF2; capture control: rabbit IgG. Results of IP were quantified by Image J, and data were presented as mean ± SD, n = 3, $^{**}p < 0.01$ *vs.* control.

(pGL4.37) and a vehicle plasmid (pGL4.75) for *ARE*-driven luciferase activities assessment. After transfection, EA.hy926 cells were treated with DMSO or Z-Lig (1–100 μM) for 24 h, respectively (Fig. 2A). EA.hy926 cells were also treated with 100 μM Z-Lig for 2, 4, 8, 12, 24 h (Fig. 2B) for luciferase activity detection. The results demonstrated that *ARE*-driven luciferase activity was increased in a dose-dependent and time-dependent pattern. The above results suggested that Z-Lig might be an inducer of the NRF2/*ARE* signaling pathway. We also found that NRF2 translocated to the nucleus in a time-dependent manner with Z-Lig treatment (Fig. 2C). Co-IP experiment showed that under 100 μm Z-Lig treatment, NRF2-KEAP1 binding complex released more free NRF2 (Fig. 2D). These results indicated that Z-Lig was a robust activator of NRF2 by promoting translocation of NRF2 from the cytoplasm to the nucleus, binding *ARE* and unbinding NRF2-KEAP1 complex.

3.3. Z-Lig increased NRF2 and ARE-driven enzyme expressions

To explore whether Z-Lig could affect expression of downstream genes of *NRF2*, cells were treated with DMSO or 1–100 μM Z-Lig for 24 h, respectively. Relative mRNA levels of *ARE*-driven antioxidant enzymes and phase II detoxifying enzymes were determined using Real-time PCR. Z-Lig dramatically stimulated the mRNA levels of *NRF2, HO-*

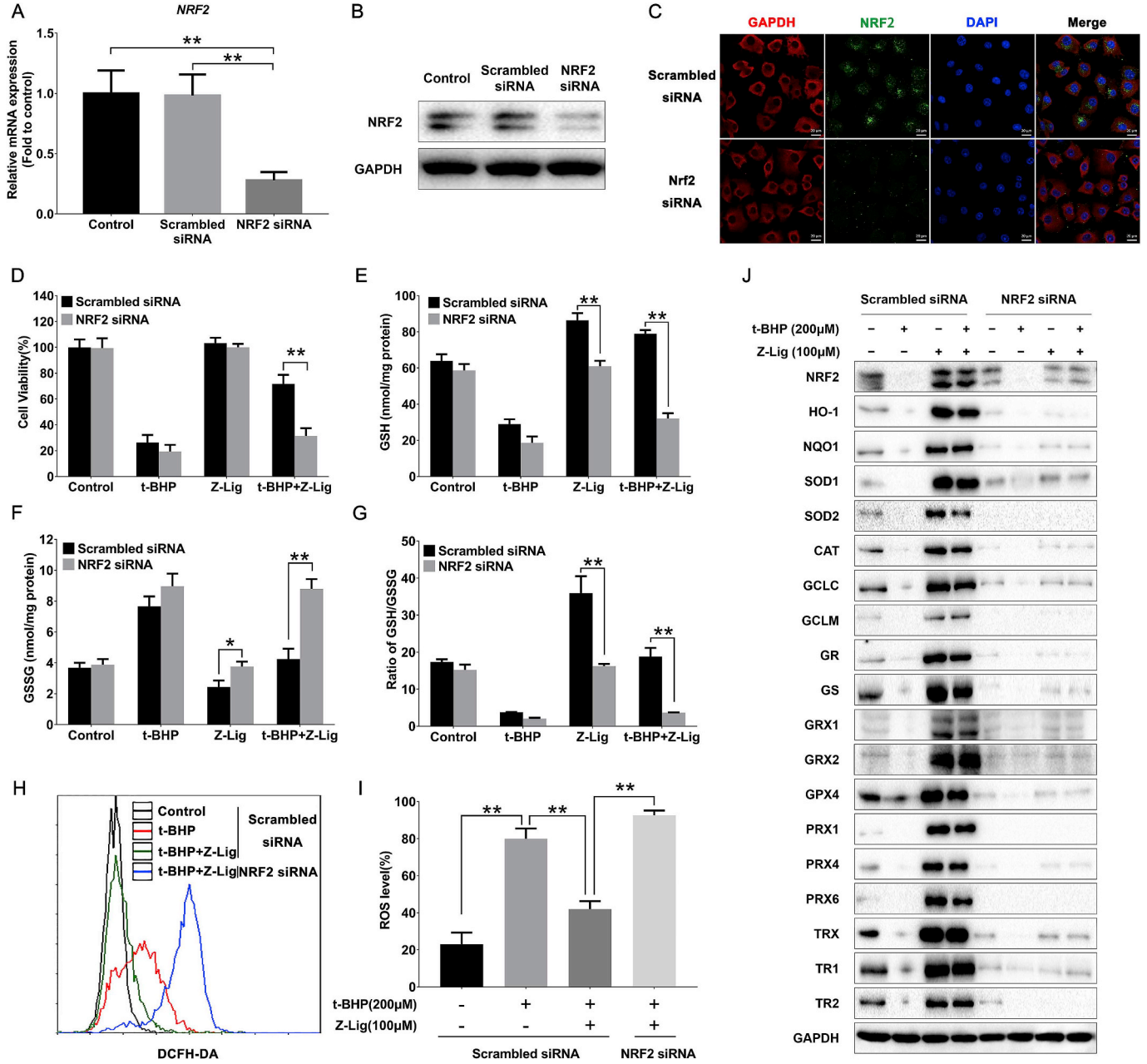

Fig. 3. *NRF2* silencing abolished Z-Lig-induced cytoprotective effects against oxidative stress and decreased the level of intracellular GSH in EA.hy926 cells. (A–C) EA.hy926 cells transfected with *NRF2* siRNA silenced *NRF2* expression in EA.hy926 cells. *NRF2* level was assayed with (A) Real-time PCR, (B) Western blotting and (C) immunofluorescence staining, respectively. Data are expressed as means ± SD (n = 3). (D–J) EA.hy926 cells were incubated with *NRF2* siRNA or scrambled siRNA. After 48 h, cells were treated with 100 μM Z-Lig for 24 h and 200 μM t-BHP for another 6 h (D, H, I) *NRF2* knockdown inhibited Z-Lig from protecting EA.hy926 cells against cell injury caused by oxidative stress. (D) Cell viability analysis. Cell viability was assayed by MTT. (H) Flow cytometry detection of intercellular ROS. (I) Quantitation of the flow cytometry data. (E–G) Effects of Z-Lig on the levels of intercellular GSH (E), GSSG (F) and the ratio of GSH/GSSG (G) in EA.hy926 cells after *NRF2* knockdown. (J) *NRF2* silencing eliminated Z-Lig-induced gene expression. The protein levels of NRF2, *NRF2*-regulated antioxidant genes were assayed by Western blotting. The values are shown as means ± SD (n = 3). $^{*}p < 0.05$ and $^{**}p < 0.01$ *vs.* control.

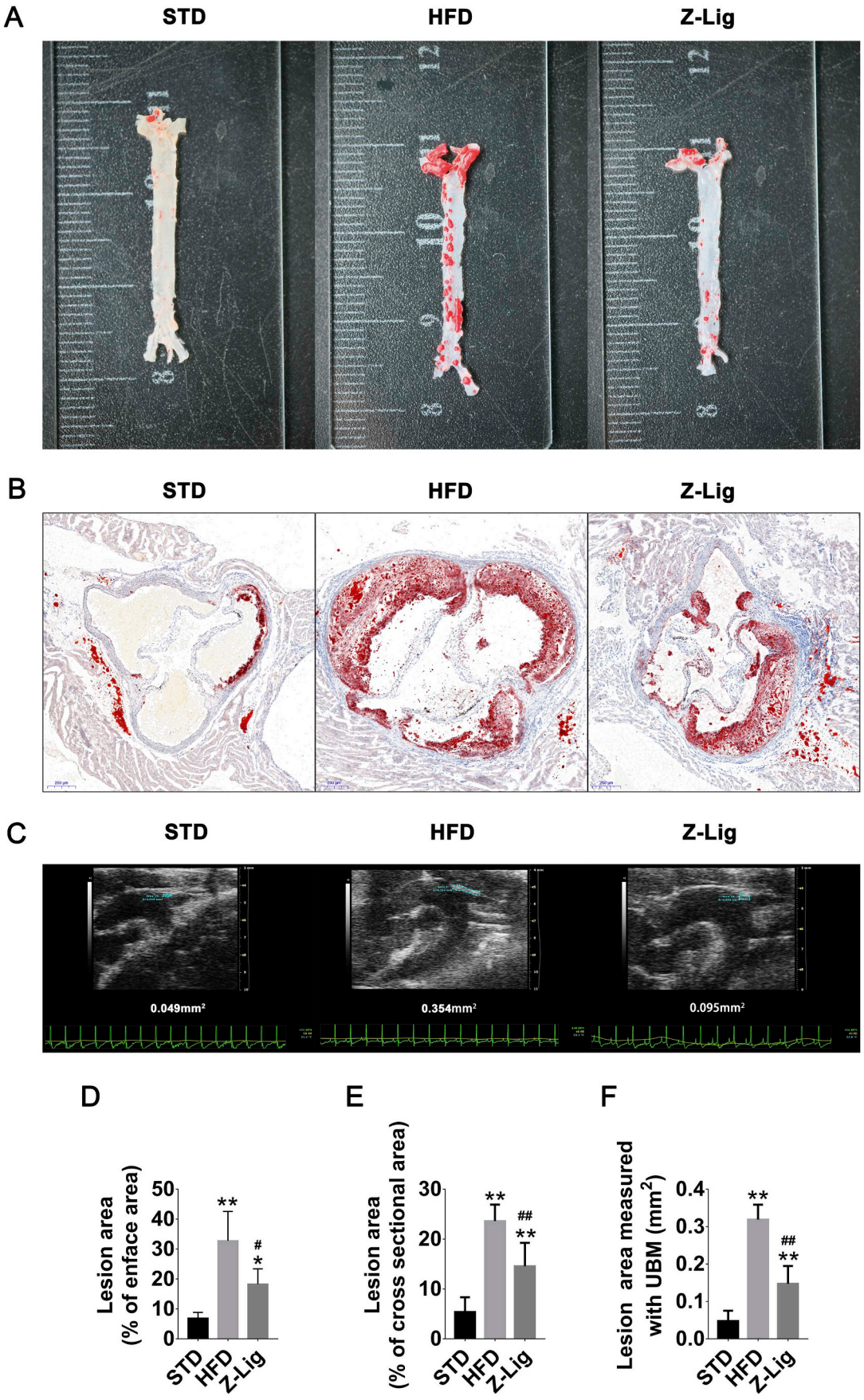

(caption on next page)

Fig. 4. Z-Lig suppressed atherosclerotic plaque formation in HFD-fed *Ldlr* $^{-/-}$ mice. (A–F) *Ldlr* $^{-/-}$ mice were treated with Z-Lig or TW − 80 for successive 8 weeks. Atherosclerotic plaques were evaluated with en face, aortic sinus sections and UBM analysis. (A) Representative images of en face ORO staining of whole aortas. (B) Representative images of aortic sinus sections stained with ORO. (C) UBM of the aortic arch in *Ldlr* $^{-/-}$ mice, showing atherosclerotic plaque with circles. Plaque areas of the aortic arch were observed at the origin of the brachiocephalic artery. (D) Quantification analysis of the atherosclerotic lesion area of the enface area (n = 5, Image-Pro Plus 6.0). (E) Quantification of atherosclerotic lesion area in cross sectional area stained with ORO (n = 5, Image-Pro Plus 6.0). (F) Statistical analysis of plaque area measured by UBM (n = 5). Values are described as mean ± SD (n = 5), $^{*}p < 0.05$, $^{**}p < 0.01$ *vs.* STD. $^{\#}p < 0.05$, $^{\#\#}p < 0.05$ *vs.* HFD.

1, NQO1, CAT, SOD1, SOD2, GCLC, GCLM, GR, GS, GPX4, GRX1, GRX2, PRX1, PRX4, PRX6, TR1, TR2, and *TRX* in a dose-dependent pattern (Supplementary Fig. 1A). Cells were then treated with 100 μM Z-Lig for 2, 4, 8, 12, 24 h, followed by mRNA level detection of these 19 genes with Real-time PCR. The results showed that Z-Lig increased the mRNA expression levels in a time-dependent manner (Supplementary Fig. 1B). Similarly, Z-Lig induced protein expression of these 19 genes in a dose- and time-dependent manner (Supplementary Figs. 1C and D). However, Z-Lig did not have significant time effects on the basal level of KEAP1 in EA.hy926 cells.

3.4. Z-Lig guarded EA.hy926 cells against t-BHP cytotoxicity via the inducement of NRF2/ARE antioxidant pathway

To investigate the potential mechanism of Z-Lig on regulating NRF2, we detected the expression of NRF2 and NRF2-mediated antioxidant genes in t-BHP-treated EA.hy926 cells. Real-time PCR and Western blotting showed that treatment with 200 μM t-BHP for 6 h significantly restrained the mRNA and protein levels of *NRF2* and its downstream genes in EA.hy926 cells, which was markedly reversed by 100 μM Z-Lig pretreatment for 24 h (Supplementary Figs. 2A and B). Moreover, immunofluorescence showed that t-BHP treatment reduced NRF2 expression and prevented nuclear accumulation of NRF2. However, intervention with 100 μM Z-Lig elevated NRF2 expression both in the cytoplasm and nucleus (marked with white arrow), which could also alleviate NRF2 suppression under t-BHP intervention (Supplementary Fig. 2C).

3.5. NRF2 silencing abolished cytoprotective effects of Z-Lig and decreased the intracellular level of GSH

To confirm whether *NRF2* was a direct target of Z-Lig, cells were transfected with specific *NRF2* siRNA and scrambled siRNA. Transfection efficacies were verified by Real-time PCR (Fig. 3A–C). Subsequently, transfected cells were treated with 100 μM Z-Lig for 24 h and 200 μM t-BHP for another 6 h, followed by detection of cell viability, intercellular levels of GSH, GSSG, ROS and expressions of Z-Lig-induced cytoprotective proteins. *NRF2* knockdown markedly abrogated the protective effect of Z-Lig on cell viability (Fig. 3D). *NRF2* depletion also sharply abolished increased GSH content, elevated ratio of GSH/GSSG and decreased GSSG content induced by Z-Lig treatment (Fig. 3E–G). In addition, increased ROS level by t-BHP stimulation was attenuated with Z-Lig treatment. However, it could be eliminated by si-*NRF2* transfection (Fig. 3H and I). Furthermore, Western blotting results showed that *NRF2* knockdown markedly impaired Z-Lig-induced upregulation of cytoprotective proteins (Fig. 3J). These data suggested cytoprotective function of Z-Lig was dependent on *NRF2* activation.

3.6. Z-Lig attenuated body weight gain, reduced serum lipid levels and alleviated HFD-induced atherosclerotic plaque formation in Ldlr $^{-/-}$ mice

Endothelial cell injury is the initial step of atherosclerosis. The present study suggested that Z-Lig protected EA.hy926 cells against oxidative damage induced by t-BHP *in vitro*. Thus, ORO staining and UBM were performed to explore the potential effects of Z-Lig on atherosclerotic lesion formation caused by HFD feeding in *Ldlr* $^{-/-}$ mice.

After HFD feeding for 8 weeks, there was no remarkable difference in food intake among the three groups (Supplementary Fig. 3). Additionally, the body weight of *Ldlr* $^{-/-}$ mice in the HFD-fed group increased significantly compared with STD, whereas administration of Z-Lig dramatically prevented body weight gain of HFD-fed *Ldlr*$^{-/-}$ mice (Supplementary Fig. 3). Moreover, serum levels of TC, TG, and LDL-C in HFD-fed *Ldlr*$^{-/-}$ mice were evidently elevated compared with those fed with STD, while HDL-C remarkably decreased (Supplementary Fig. 3). However, after 8-week treatment with Z-Lig, a significant rescue in serum levels of TC, TG, LDL-C and HDL-C was observed (Supplementary Fig. 3).

ORO staining indicated that HFD feeding dramatically increased atherosclerotic plaque area, whereas Z-Lig treatment obviously mitigated HFD induced-atherosclerotic lesion formation in the *en face* prepared aorta (Fig. 4A and D) and aortic sinus (Fig. 4B and E) of *Ldlr*$^{-/-}$ mice. Moreover, we measured the plaque areas at the origin of the brachiocephalic artery with UBM. Mice treated with Z-Lig displayed markedly reduced plaque areas compared with those with only HFD feeding (Fig. 4C and F). Collectively, these data suggested that Z-Lig prevented *Ldlr*$^{-/-}$ mice from atherosclerotic plaque formation induced by HFD feeding.

3.7. Z-Lig attenuated lipid peroxidation, increased GSH/GSSG level and antioxidant enzyme activity of Ldlr $^{-/-}$ mice

Lipid peroxidation is believed to be a crucial step in the pathogenesis of atherosclerosis [28]. Therefore, lipid peroxidation levels in aortas of *Ldlr* $^{-/-}$ mice were measured. After HFD feeding for 8 weeks, MDA content in the serum and aortas (Supplementary Fig. 4A andB) as well as 4-Hne expression in the vascular endothelium and aortas (Fig. 5A and Supplementary Fig. 5A) of *Ldlr* $^{-/-}$ mice significantly increased compared with those fed with STD. However, after 8-week treatment with Z-Lig, a significant rescue in MDA content (Supplementary Fig. 4A and B) and 4-Hne expression (Figs. 5A and S5A) was observed. Additionally, Z-Lig intervention remarkably elevated GSH/GSSG level (Supplementary Fig. 4I-N) and activities of Sod, Cat and Gpx in serum and aortas of *Ldlr* $^{-/-}$ mice (Supplementary Figs. 4C–H).

3.8. Z-Lig activated Nrf2, stimulated Nrf2 nuclear accumulation and increased Nrf2 downstream gene expressions in vascular endothelium and aortas of Ldlr $^{-/-}$ mice

Expressions of Nrf2 and selected Nrf2-mediated genes in aortas of *Ldlr* $^{-/-}$ mice were determined by Western Blotting (Fig. 5A), immunofluorescence staining (Fig. 5B) and immunohistochemistry staining (Supplementary Figs. 5B–F) respectively. Protein expressions of Nrf2 and the selected Nrf2 downstream genes in vascular endothelium and aortas were remarkably upregulated with Z-Lig intervention. Moreover, Nrf2 nuclear accumulation in vascular endothelium and aortas remarkably increased upon Z-Lig treatment (Fig. 5B and Supplementary 5B). These results were consistent with the *in vitro* data, demonstrating that the protective effects of Z-Lig against atherosclerotic plaque formation was associated with Nrf2/*ARE* signaling pathway in vascular endothelium.

4. Discussion

In this study, we have demonstrated, for the first time, that Z-Lig

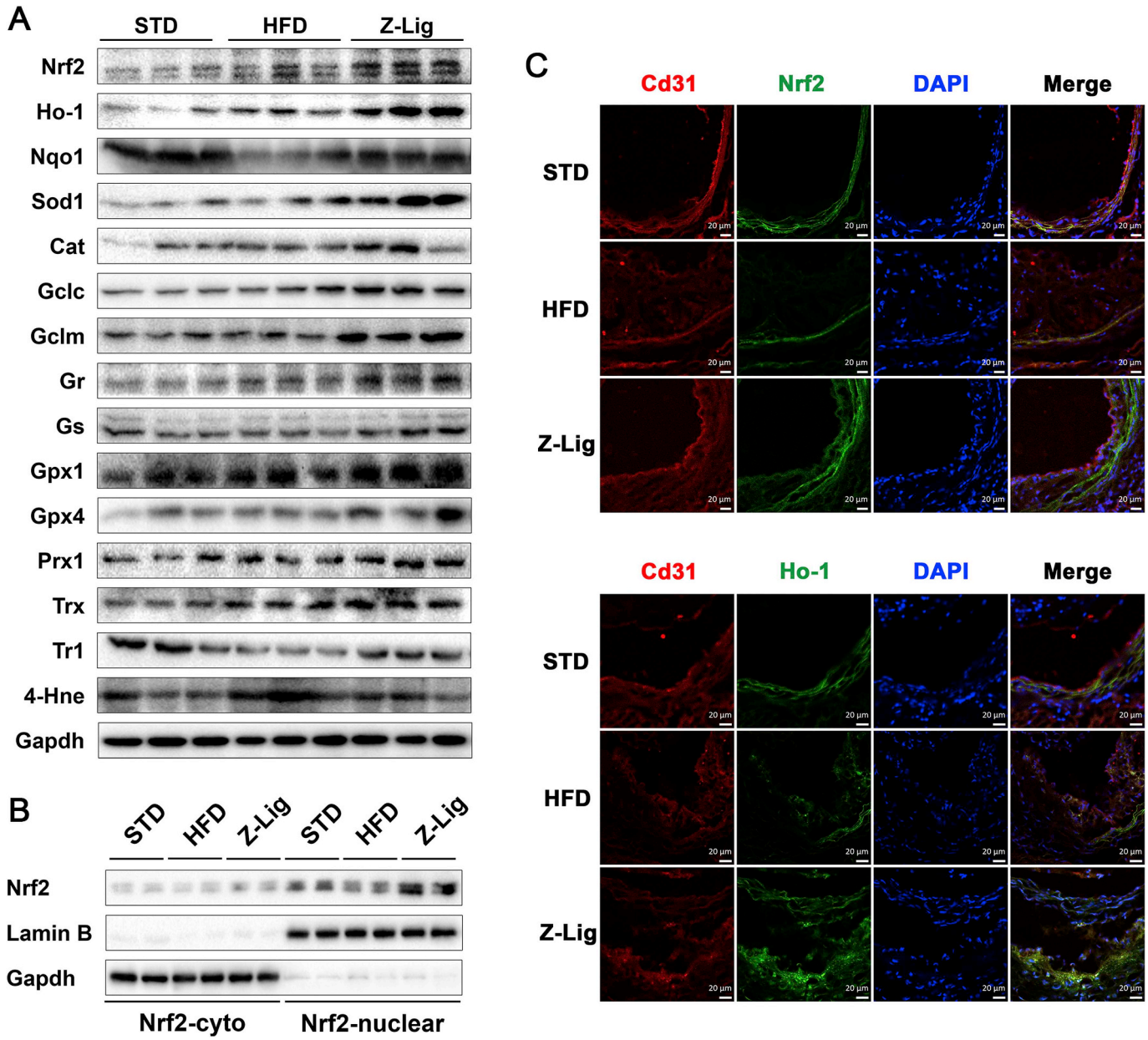

Fig. 5. Z-Lig activated Nrf2, stimulated Nrf2 nulear accumulation, increased *Nrf2* downstream gene expression and suppressed 4-Hne expression in vascular endothelium and aortas of *Ldlr* $^{-/-}$ mice.

(A) Z-Lig increased protein levels of Nrf2 and *Nrf2* downstream genes and suppressed 4-Hne expression in aortas of *Ldlr* $^{-/-}$ mice. Protein expression was detected by Western Blotting. Representative results were from three mice per group. (B) Z-Lig promoted accumulation of nuclear Nrf2 in aortas of *Ldlr* $^{-/-}$ mice. Western Blotting was applied to detect protein expression of Nrf2 in nucleus and cytoplasm. Representative results were from two mice per group. (C) Representative images of immunofluorescence staining. Co-stained for Nrf2 and its downstream targets (Nrf2 and Ho-1; green), endothelial cells (ECs) (Cd-31; red), and nuclei (DAPI; blue). Scale bar = 20 μm. (For interpretation of the references to colour in this figure legend, the reader is referred to the Web version of this article.)

alleviated oxidative stress caused by t-BHP in EA.hy926 cells. Z-Lig also ameliorated endothelial dysfunction and atherosclerotic plaque formation in HFD-fed *Ldlr* $^{-/-}$ mice. The specific role of Z-Lig was associated with activation of the NRF2/*ARE* signaling pathway.

Excessive ROS production plays a great part in the pathogenesis of endothelial dysfunction [29,30]. There are numerous studies suggesting a vital role of Z-Lig on cytoprotection and antioxidation [31–33]. Previous studies have reported that Z-Lig reduced intracellular ROS production, suppressed ROS-induced cell injury, and induced GSH production [24,25]. In this study, we found that t-BHP markedly raised intracellular ROS and GSSG levels, while significantly decreased cell viability, intracellular GSH content and the ratio of GSH/GSSG. However, preincubation with Z-Lig markedly attenuated the t-BHP-induced elevation of ROS and GSSG, and dramatically rescued the decreased levels of cell viability, GSH and GSH/GSSG. The human endothelial cell line EA.hy926 has been widely used in studies on differentiated endothelial cell functions such as angiogenesis, inflammation and oxidative stress [34–36]. Using the EA.hy926 cell line, we investigated the potential molecular mechanisms associated with the cytoprotective and antioxidant effects of Z-Lig, lying emphasis on *ARE* activation. In the present work, we found that Z-Lig acted as an *ARE* inducer in a dose- and time-dependent pattern. Numerous studies have indicated that *ARE* sequences regulate expressions of various antioxidant genes. Besides, NRF2 acts as a primary regulator of the *ARE*-mediated cellular guard system against excessive ROS production [37–39]. NRF2 is degraded in the cytoplasm by KEAP1-CULLIN3 ubiquitination system under normal

conditions. Some redox-active components, protein kinase, epigenetic factors and other *ARE* activation signals may disrupt the KEAP1-CULLIN3 combination, thus promoting translocation of NRF2 into the nucleus. Nuclear NRF2 binds to *ARE*, resulting in induction of *ARE*-driven genes [40,41]. We reported in this study that NRF2 expression in EA.hy926 cell line was induced by Z-Lig in a dose- and time-dependent mode. Z-Lig also allowed nuclear translocation of NRF2 in a time-dependent manner. In addition, Z-Lig promoted NRF2/KEAP1 complex unbinding, which increased the content of free NRF2 in the cytoplasm. It is reported that Z-Lig can alkylate an important cysteine residue (Cys151) in KEAP1, which can lead to dissociation of KEAP1-NRF2 and stimulate the accumulation of NRF2 in the nucleus [42]. The mechanism linking Z-Lig to KEAP1-NRF2 dissociation may be related to the alkylation modification of KEAP1.

The NRF2/*ARE* pathway regulates hundreds of antioxidant and detoxifying enzymes [12,14]. GCLC, GCLM, GS, GR, and GPXs contribute to GSH biosynthesis and metabolism [43]. GSH biosynthesis needs two ATP-dependent steps. The first step is mediated by GCLC and GCLM, and the second step is regulated by GS [44]. ROS sources increase the level of hydrogen peroxide (H_2O_2). GPXs detoxify H_2O_2 by converting 2 GSH molecules to its oxidized form GSSG, which in turn is reduced back to GSH by GR to create a redox cycle [44,45]. Interconnection of GRX, PRX, TRX, TR, and GSH builds the antioxidant systems [43]. H_2O_2 can be reduced by PRX or GPX. GPXs couple oxidation of GSH with detoxification of H_2O_2 [46]. PRXs are thiol-specific proteins that react with H_2O_2 at a very high rate, which can also reduce and detoxify peroxynitrite and a wide range of organic hydroperoxides [47–49]. Oxidized cysteine residues of PRX are specifically reduced by TRX, thiol-disulfide oxidoreductases that can be oxidized upon oxidative stress caused by a variety of stimuli [50]. Subsequently, oxidized TRX is reduced by TR in a NADPH-dependent manner [50]. Moreover, GSH is also a cofactor and substrate for GRXs that catalyzes disulfide reductions in the presence of NADPH and GR [51]. Superoxide (O_2^-) is produced as a by-product of oxygen metabolism and, if not regulated, causes many types of cell damage [52]. SODs and CAT are both common enzymes found in nearly all living organisms exposed to oxygen. SODs are enzymes that alternately catalyze the dismutation (or partitioning) of the superoxide radical into either ordinary molecular oxygen (O_2) or H_2O_2. H_2O_2 is then converted by CAT to oxygen and water [53,54]. HO-1, encoded by the *HMOX1* gene, can convert heme into the powerful pro-oxidant biliverdin, which is then transformed into bilirubin, a strong antioxidant [55]. NQO1 encodes a cytoplasmic 2-electron reductase. This FAD-binding protein forms homodimers and reduces quinones to hydroquinones. Enzymatic activity of NQO1 prevents the one electron reduction of quinones that results in the production of radical species [56]. HO-1, NQO1 and GPXs are considered as the most important targets of NRF2, which are involved in the reduction of oxidative damage in the endothelium or arteries during the atheroprotective process [57,58]. In the present work, we tested the impact of Z-Lig on the levels of 26 antioxidant enzymes. After EA.hy926 cells were treated with different doses of Z-Lig for different time points, we observed that Z-Lig significantly increased mRNA and protein expressions of 18 ARE-driven genes in EA.hy926 cells in a dose and time-dependent pattern (*HO-1, NQO1, SOD1/2, CAT, GCLC, GCLM, GS, GR, GPX4, GRX1/2, PRX1/4/6, TR1/2* and *TRX*). We also investigated the effects of Z-Lig on 18 ARE-mediated genes in t-BHP-challenged EA.hy926 cells. Our data suggested that t-BHP treatment in EA.hy926 cells markedly suppressed the expressions of NRF2 and 18 ARE-driven enzymes, whereas pretreatment with Z-Lig still strongly stimulated the mRNA and protein expressions of the 19 genes. Furthermore, we silenced *NRF2* with a specific siRNA to identify the role of NRF2 in Z-Lig-activated upregulation of 18 ARE-driven genes. *NRF2* knockdown markedly inhibited the upregulation induced by Z-Lig treatment, indicating that Z-Lig activated NRF2-*ARE* signal axis under oxidative stress.

Oxidative stress generating from excessive ROS production results in impaired endothelial function, which promotes atherosclerotic lesion or foam cell formation [59,60]. Therefore, to further investigate the chemopreventive effects of Z-Lig on oxidative stress-induced endothelial dysfunction and atherosclerosis *in vivo*, *Ldlr* $^{-/-}$ mice were supplemented with HFD and Z-Lig for successive 8 weeks. *Ldlr* $^{-/-}$ mice have been widely used as a model to mimic human atherosclerosis. HFD leads to hyperlipidemia lipid peroxidation and atherosclerotic lesion development [61]. It was observed that Z-Lig exerted protective effects on attenuating body weight gain, reducing serum lipid levels, alleviating atherosclerotic plaque formation, decreasing lipid peroxidation and increasing antioxidant enzyme activity in HFD-fed *Ldlr* $^{-/-}$ mice. Furthermore, Western blotting, immunohistochemical and immunofluorescence staining results indicated the chemopreventive effects of Z-Lig might be associated with the activation of NRF2 and *ARE*-driven genes.

Nevertheless, some limitations of our study must be pointed out. GSTs, another important phase II detoxifying enzyme family with 22 family members in humans, have not been taken into consideration in this study. Moreover, the effects of Z-Lig-induced GSH biosynthesis on protecting EA.hy926 cells from oxidative and cell injury have not been elucidated. In addition, *Ldlr* $^{-/-}$ or *Apoe* $^{-/-}$ mice with endotheliocyte-selective deletion of *Nrf2* should be applied to further evaluate the endothelial protection function of Z-Lig through inhibiting Nrf2 pathway directly. Further in-depth researches should be carried out to explore the abovementioned limitations.

In conclusion, our study demonstrated for the first time that Z-Lig elevates the expressions of various antioxidant genes and suppress ROS production through NRF2 activation in EA.hy926 cells. Moreover, Z-Lig might exert a great influence on defending against endothelial dysfunction and relieving atherosclerotic plaque formation via Nrf2 pathway in HFD-fed mice. Our work demonstrated that Z-Lig might be therapeutic target for the management of atherosclerotic CHD.

Conflicts of interest

The authors declared they do not have anything to disclose regarding conflict of interest with respect to this manuscript.

Author contributions

N. G. and W.-M. J. designed the experiments and contributed reagents/materials/analysis tools; Y. Z., Y.-J. Z., X. H., Y. X., Y. Q. and H.-Y. L. performed the experiments and wrote the paper. All authors participated in collecting and analyzing data and preparing the manuscript and approved the final version of the manuscript for publication.

Financial support

This work was supported by National Natural Science Foundation of China (Grant No. 81373605, 81774229 and 81173399), Natural Science Foundation of Jiangsu Province, China (Grant No.BK20161115 and BK20181503), the project of medical science and technology innovation platform in 13th Five-Year Plan (Nanjing Health and Family Planning Commission, ZDX16009).

Appendix A. Supplementary data

Supplementary data to this article can be found online at https://doi.org/10.1016/j.atherosclerosis.2019.02.010.

References

[1] A. Bhatnagar, Environmental Basis of Cardiovascular Disease, Environmental Cardiology (2010) 1–75.
[2] J.I. Kim, A. Sillah, J.L. Boucher, A.C. Sidebottom, T. Knickelbine, Prevalence of the American Heart Association's "ideal cardiovascular health" metrics in a rural, cross-

sectional, community-based study: the Heart of New Ulm Project, Journal of the American Heart Association Cardiovascular & Cerebrovascular Disease 2 (3) (2013) e000058-e000058.
[3] I.S. Vujcic, S.B. Sipetic, E.S. Dubljanin, H.D. Vlajinac, Trends in mortality rates from coronary heart disease in Belgrade (Serbia) during the period 1990–2010: a join-point regression analysis, BMC Cardiovasc. Disord. 13 (1) (2013) 112.
[4] U. Förstermann, Nitric oxide and oxidative stress in vascular disease, Pflügers Archiv 459 (6) (2010) 923–939.
[5] U. Laufs, S. Wassmann, T. Czech, T. Münzel, M. Eisenhauer, M. Böhm, G. Nickenig, Physical inactivity increases oxidative stress, endothelial dysfunction, and atherosclerosis, Arterioscler. Thromb. Vasc. Biol. 25 (4) (2005) 809–814.
[6] V. VM, R. M, S. E, B. C, G.-M. K, H.-M. A, Oxidative stress, endothelial dysfunction and atherosclerosis, Curr. Pharmaceut. Des. 15 (26) (2009) 2988–3002.
[7] K. Uno, S.J. Nicholls, Biomarkers of inflammation and oxidative stress in atherosclerosis, Biomark. Med. 4 (3) (2017) 361–373.
[8] M.L. Circu, T.Y. Aw, Reactive oxygen species, cellular redox systems, and apoptosis, Free Radical Biol. Med. 48 (6) (2010) 749.
[9] X. Liu, K. Ward, C. Xavier, J. Jann, A.F. Clark, I.H. Pang, H. Wu, The novel triterpenoid RTA 408 protects human retinal pigment epithelial cells against H2O2-induced cell injury via NF-E2-related factor 2 (Nrf2) activation, Redox Biology 8 (C) (2015) 98.
[10] S. Jeayeng, A. Wongkajornsilp, A.T. Slominski, S. Jirawatnotai, S. Sampattavanich, U. Panich, Nrf2 in keratinocytes modulates UVB-induced DNA damage and apoptosis in melanocytes through MAPK signaling, Free Radical Biol. Med. 108 (2017) 918–928.
[11] K. Yama, K. Sato, N. Abe, M. Yu, R. Tatsunami, Y. Tampo, Epalrestat increases glutathione, thioredoxin, and heme oxygenase-1 by stimulating Nrf2 pathway in endothelial cells, Redox Biology 4 (C) (2015) 87.
[12] C. Bo, Y. Lu, Y. Chen, J. Cheng, The role of Nrf2 in oxidative stress-induced endothelial injuries, J. Endocrinol. 225 (3) (2015) 83–99.
[13] C. Espinosa-Diez, V. Miguel, D. Mennerich, T. Kietzmann, P. Sánchez-Pérez, S. Cadenas, S. Lamas, Antioxidant responses and cellular adjustments to oxidative stress, Redox Biology 6 (2015) 183–197.
[14] A.K. Jaiswal, Nrf2 signaling in coordinated activation of antioxidant gene expression, Free Radical Biol. Med. 36 (10) (2004) 1199–1207.
[15] A. Ishikado, Y. Sono, M. Matsumoto, S. Robidastubbs, A. Okuno, M. Goto, G.L. King, T.K. Blackwell, T. Makino, Willow bark extract increases antioxidant enzymes and reduces oxidative stress through activation of Nrf2 in vascular endothelial cells and Caenorhabditis elegans, Free Radical Biol. Med. 65 (4) (2012) 1506–1515.
[16] Y. Zhu, Salidroside suppresses HUVECs cell injury induced by oxidative stress through activating the Nrf2 signaling Pathway, 21 (8) (2016).
[17] Y. Yang, X. Cai, J. Yang, X. Sun, C. Hu, Z. Yan, X. Xu, W. Lu, X. Wang, P. Cao, Chemoprevention of dietary digitoflavone on colitis-associated colon tumorigenesis through inducing Nrf2 signaling pathway and inhibition of inflammation, Mol. Canc. 13 (1) (2014) 48.
[18] Y. Ding, B. Zhang, K. Zhou, M. Chen, M. Wang, Y. Jia, Y. Song, Y. Li, A. Wen, Dietary ellagic acid improves oxidant-induced endothelial dysfunction and atherosclerosis: role of Nrf2 activation, Int. J. Cardiol. 175 (3) (2014) 508–514.
[19] L. Xie, Y. Gu, M. Wen, S. Zhao, W. Wang, Y. Ma, G. Meng, Y. Han, Y. Wang, G. Liu, Hydrogen sulfide induces Keap1 S-sulfhydration and suppresses diabetes-accelerated atherosclerosis via Nrf2 activation, Diabetes 65 (10) (2016) 3171.
[20] A.K. Ruotsalainen, M. Inkala, M.E. Partanen, J.P. Lappalainen, E. Kansanen, P.I. Mäkinen, S.E. Heinonen, H.M. Laitinen, J. Heikkilä, T. Vatanen, The absence of macrophage Nrf2 promotes early atherogenesis, Cardiovasc. Res. 98 (1) (2013) 107.
[21] P.O. Donkor, Y. Chen, L. Ding, F. Qiu, Locally and traditionally used Ligusticum species - a review of their phytochemistry, pharmacology and pharmacokinetics, J. Ethnopharmacol. 194 (2016) 530–548.
[22] A.H. Zuo, L. Wang, H.B. Xiao, Research progress studies on pharmacology and pharmacokinetics of ligustilide, China J. Chin. Mater. Med. 37 (22) (2012) 3350.
[23] W.L. Wei, R. Zeng, C.M. Gu, Y. Qu, L.F. Huang, Angelica sinensis in China-A review of botanical profile, ethnopharmacology, phytochemistry and chemical analysis, J. Ethnopharmacol. 190 (2016) 116–141.
[24] Z. Wu, H. Uchi, S. Morino-Koga, W. Shi, M. Furue, Z-ligustilide ameliorated ultraviolet B-induced oxidative stress and inflammatory cytokine production in human keratinocytes through upregulation of Nrf2/HO-1 and suppression of NF-κB pathway, Exp. Dermatol. 24 (9) (2015) 703–708.
[25] H. Qi, Y. Han, J. Rong, Potential roles of PI3K/Akt and Nrf2–Keap1 pathways in regulating hormesis of Z-ligustilide in PC12 cells against oxygen and glucose deprivation, Neuropharmacology 62 (62) (2012) 1659–1670.
[26] J. Li, J. Yu, H. Ma, N. Yang, L. Li, D. Zheng, M. Wu, Z. Zhao, H. Qi, Intranasal pretreatment of Z-ligustilide, the main volatile component of rhizoma chuanxiong, confers prophylaxis Against cerebral ischemia via Nrf2 and HSP70 signaling pathway, J. Agric. Food Chem. 65 (8) (2017).
[27] X. Feng, W. Yu, X. Li, F. Zhou, W. Zhang, Q. Shen, J. Li, C. Zhang, P. Shen, Apigenin, a modulator of PPARγ, attenuates HFD-induced NAFLD by regulating hepatocyte lipid metabolism and oxidative stress via Nrf2 activation, Biochem. Pharmacol. 136 (2017).
[28] L. Nagy, Oacute, G. Spiteller, Atherosclerosis and lipid peroxidation, Mol. Nutr. Food Res. 49 (11) (2010) 989–991.
[29] M.A. Incalza, R. D'Oria, A. Natalicchio, S. Perrini, L. Laviola, F. Giorgino, Oxidative Stress and Reactive Oxygen Species in Endothelial Dysfunction Associated with Cardiovascular and Metabolic Diseases, Vascular Pharmacology, 2017.
[30] H. Cai, D.G. Harrison, Endothelial dysfunction in cardiovascular diseases: the role of oxidant stress, Circ. Res. 87 (10) (2000) 840–844.
[31] Z. W, H. U, S. Morino-Koga, A. Nakamura-Satomura, K. Kita, W. Shi, M. Furue, Z-Ligustilide inhibits benzo(a)pyrene-induced CYP1A1 upregulation in cultured human keratinocytes via ROS-dependent Nrf2 activation, Exp. Dermatol. 23 (4) (2014) 260–265.
[32] H. Qi, J. Rong, Z-ligustilide protects neuronal PC12 cells from oxidative stress by inducing heme oxygenase-1 via the Nrf2 and PI3K/Akt mediated pathways, Inorg. Chem. 52 (5) (2010) 2564–2580.
[33] B. Peng, P. Zhao, Y.P. Lu, M.M. Chen, H. Sun, X.M. Wu, L. Zhu, Z-ligustilide activates the Nrf2/HO-1 pathway and protects against cerebral ischemia-reperfusion injury in vivo and in vitro, Brain Res. 1520 (32) (2013) 168–177.
[34] K. Zhao, X. Li, B. Lin, D. Yang, Y. Zhou, Z. Li, Q. Guo, N. Lu, Oroxyloside inhibits angiogenesis through suppressing internalization of VEGFR2/Flk-1 in endothelial cells, J. Cell. Physiol. 233 (4) (2017) 3454–3464.
[35] S.P. Deakin, S. Bioletto, M.-L. Bochaton-Piallat, R.W. James, HDL-associated paraoxonase-1 can redistribute to cell membranes and influence sensitivity to oxidative stress, Free Radic. Biol. Med. 50 (1) (2011) 102–109.
[36] C.-Y. Chao, C.-K. Lii, I.-T. Tsai, C.C. Li, K.-L. Liu, C.-W. Tsai, H.-W. Chen, Andrographolide inhibits ICAM-1 expression and NF-κB activation in TNF-α-treated EA. hy926 cells, J. Agric. Food Chem. 59 (10) (2011) 5263–5271.
[37] A.K. Jaiswal, Nrf2 signaling in coordinated activation of antioxidant gene expression, Free Radic. Biol. Med. 36 (10) (2004) 1199–1207.
[38] T. Nguyen, P. Nioi, C.B. Pickett, The Nrf2-antioxidant response element signaling pathway and its activation by oxidative stress, J. Biol. Chem. 284 (20) (2009) 13291–13295.
[39] K. Itoh, T. Chiba, S. Takahashi, T. Ishii, K. Igarashi, Y. Katoh, T. Oyake, N. Hayashi, K. Satoh, I. Hatayama, An Nrf2/small Maf heterodimer mediates the induction of phase II detoxifying enzyme genes through antioxidant response elements, Biochem. Biophys. Res. Commun. 236 (2) (1997) 313–322.
[40] H.K. Bryan, A. Olayanju, C.E. Goldring, B.K. Park, The Nrf2 cell defence pathway: keap1-dependent and -independent mechanisms of regulation, Biochem. Pharmacol. 85 (6) (2013) 705–717.
[41] M.C. Jaramillo, D.D. Zhang, The emerging role of the Nrf2-Keap1 signaling pathway in cancer, Genes Dev. 27 (20) (2013) 2179–2191.
[42] B.M. Dietz, D. Liu, G.K. Hagos, P. Yao, A. Schinkovitz, S.M. Pro, S. Deng, N.R. Farnsworth, G.F. Pauli, R.B. Van Breemen, Angelica sinensis and its alkylphthalides induce the detoxification enzyme NAD (P) H: quinone oxidoreductase 1 by alkylating Keap1, Chem. Res. Toxicol. 21 (10) (2008) 1939–1948.
[43] C. Espinosadiez, V. Miguel, D. Mennerich, T. Kietzmann, P. Sánchezpérez, S. Cadenas, S. Lamas, Antioxidant responses and cellular adjustments to oxidative stress, Redox Biology 6 (2015) 183–197.
[44] S.C. Lu, Glutathione synthesis, Biochim. Biophys. Acta Gen. Subj. 1830 (5) (2013) 3143–3153.
[45] S.C. Lu, Regulation of glutathione synthesis, Mol Aspects Med, Molecular Aspects of Medicine 30 (1–2) (2008) 42–59.
[46] J.L. Edith Lubos, Diane E. Handy, Glutathione peroxidase-1 in health and disease: from molecular mechanisms to therapeutic opportunities, Antioxidants Redox Signal. 15 (7) (2011) 1957–1997.
[47] Z.A. Wood, E. Schröder, H.J. Robin, L.B. Poole, Structure, mechanism and regulation of peroxiredoxins, Trends Biochem. Sci. 28 (1) (2003) 32.
[48] Z.A. Wood, L.B. Poole, P.A. Karplus, Peroxiredoxin evolution and the regulation of hydrogen peroxide signaling, Science 300 (5619) (2003) 650–653.
[49] J. Fujii, Y. Ikeda, Advances in our understanding of peroxiredoxin, a multifunctional, mammalian redox protein, Redox Rep. 7 (3) (2002) 123–130.
[50] A. Holmgren, C. Johansson, C. Berndt, M.E. Lönn, C. Hudemann, C.H. Lillig, Thiol redox control via thioredoxin and glutaredoxin systems, Biochem. Soc. Trans. 33 (Pt 6) (2005) 1375.
[51] A.P. Fernandes, A. Holmgren, Glutaredoxins: glutathione-dependent redox enzymes with functions far beyond a simple thioredoxin backup system, Antioxidants Redox Signal. 6 (1) (2004) 63.
[52] M. Hayyan, M.A. Hashim, I.M. Alnashef, Superoxide ion: generation and chemical implications, Chem. Rev. (2016) 3029–3085.
[53] J.M. Mccord, I. Fridovich, Superoxide dismutases: you've come a long way, baby, Antioxidants Redox Signal. 20 (10) (2014) 1548–1549.
[54] P. Chelikani, I. Fita, P.C. Loewen, Diversity of structures and properties among catalases, Cellular & Molecular Life Sciences Cmls 61 (2) (2004) 192–208.
[55] M. Mishra, J.F. Ndisang, A critical and comprehensive insight on heme oxygenase and related products including carbon monoxide, bilirubin, biliverdin and ferritin in type-1 and type-2 diabetes, Curr. Pharmaceut. Des. 20 (9) (2014) 1370–1391.
[56] D. Ross, NQO1 (NAD(P)H Dehydrogenase, Quinone 1), (2004).
[57] T. Van-Assche, V. Huygelen, M.J. Crabtree, C. Antoniades, Gene therapy targeting inflammation in atherosclerosis, Curr. Pharmaceut. Des. 17 (37) (2011) 4210–4223.
[58] B. Buijsse, D.H. Lee, L. Steffen, R.R. Erickson, R.V. Luepker, J.D. Jr, J.L. Holtzman, Low serum glutathione peroxidase activity is associated with increased cardiovascular mortality in individuals with low HDLc's, PLoS One 7 (6) (2012) e38901.
[59] F.J. Pashkow, Oxidative stress and inflammation in heart disease: do antioxidants have a role in treatment and/or prevention? Int. J. Inflamm. 2011 (1) (2011) 514623.
[60] D.P. Hajjar, A.M. Gotto Jr., Biological relevance of inflammation and oxidative stress in the pathogenesis of arterial diseases, Am. J. Pathol. 182 (5) (2013) 1474–1481.
[61] Y. Ma, W. Wang, J. Zhang, Y. Lu, W. Wu, H. Yan, Y. Wang, Hyperlipidemia and atherosclerotic lesion development in Ldlr-deficient mice on a long-term high-fat diet, PLoS One 7 (4) (2012) e35835.